Theoretical analysis of the onset of liquid entrainment for slots of finite width

H. M. Soliman and G. E. Sims
Department of Mechanical and Industrial Engineering, University of Manitoba, Winnipeg, Manitoba, Canada

The onset of liquid entrainment during discharge from large reservoirs containing a stratified mixture of two immiscible fluids through a side slot of a finite width is considered theoretically. A previously reported analysis in which the slot was approximated as a two-dimensional line sink has been extended to account for the finite width of the slot. The model resulting from the present analysis is expressed in terms of two simple algebraic equations suitable for hand calculations. According to the present results, the ratio of the critical height to the slot width is dependent only on the Froude number. Numerical results show that the present model approaches the correct physical limits at low Froude numbers and it converges to the predictions of the previously reported simple model at high Froude numbers.

Keywords: liquid entrainment; incipience; side slots; theoretical prediction

Introduction

The development of experimental correlations and theoretical models for the accurate prediction of the flow rate and quality during two-phase discharge through small breaks in pipes has received considerable attention in the recent literature. This interest is due to the relevance of this topic to nuclear reactor safety in connection with postulated loss of coolant accidents. Two important phenomena were identified by Zuber[1] that can have a strong influence on the discharging flow through breaks; these are liquid entrainment and gas pull-through. Empirical formulas correlating the onsets of these two phenomena were reported recently[2–6] for different break orientations, flow rates, and gas–liquid combinations. As well, theoretical models were developed for the prediction of discharge flow rate and quality.[7,8] All the results reported[2–8] correspond to breaks that can be simulated as circular orifices.

In the present investigation, the onset of liquid entrainment during discharge from large reservoirs through side slots is considered analytically. This break geometry is of significant practical importance (e.g., longitudinal cracks in pipes); however, so far, it has received limited attention. The flow situation, shown schematically in Figure 1, considers a stratified mixture of two immiscible fluids (densities ρ and $\rho + \Delta\rho$) contained in a large reservoir with a horizontal slot of width d in the vertical wall of the reservoir. This slot is located in the region of the wall adjacent to the lighter fluid. If a discharge of a rate q per unit slot length is induced while the distance between the slot's centerline and the interface is sufficiently large, only the lighter fluid will be present in the discharging flow and the whole interface will be flat. By gradually decreasing the height of the slot's centerline, the interface gradually deflects upward in the vicinity of the wall until a critical height h is reached where traces of the heavier fluid are detected in the discharging flow. This incidence is referred to as the onset of liquid entrainment and the objective of this investigation is to develop a theoretical correlation for h as a function of q, d, and other relevant parameters.

The only other theoretical investigation of the problem posed is the one reported by Craya.[9] In his simplified analysis, Craya simulated the slot as a two-dimensional (2-D) line sink and obtained the following correlations:

$$h/d = 0.699\ \mathrm{Fr}^{2/3} \tag{1}$$

and

$$s = 2h/3 \tag{2}$$

where s is the distance between the tip of the deflected interface and the slot's centerline (Figure 1), and Fr is Froude number given by

$$\mathrm{Fr} = \frac{V_d}{\sqrt{dg\,\Delta\rho/\rho}} \tag{3a}$$

with

$$V_d = q/d \tag{3b}$$

It is evident that Equations 1 and 2 do not reach the appropriate limits as Fr approaches zero. At the limit Fr = 0, these equations give $h = s = 0$, while the physics of the problem suggests $h = s = d/2$ at this limit. Therefore, the accuracy of Equations 1 and 2 is doubtful at low values of Fr and this behavior is attributed to the line-sink assumption used elsewhere.[9] In the present study, a more complete analysis is developed, taking into consideration the finite size of the slot, thus making the results applicable to the whole range of Fr.

Analysis

In the present flow situation, the lighter fluid is in motion while the heavier fluid is at rest. The dominant forces are the inertia and gravity forces, while the effects of viscosity and surface tension are assumed to be negligible. Steady, incompressible, potential flow is assumed in the lighter fluid, and equilibrium of the interface is controlled by a balance between inertia and gravity forces. In determining the onset of liquid entrainment,

Address reprint requests to Dr. Soliman at the Department of Mechanical and Industrial Engineering, University of Manitoba, Winnipeg, Manitoba, Canada R3T 2N2.

Received 27 January 1991; accepted 31 May 1991

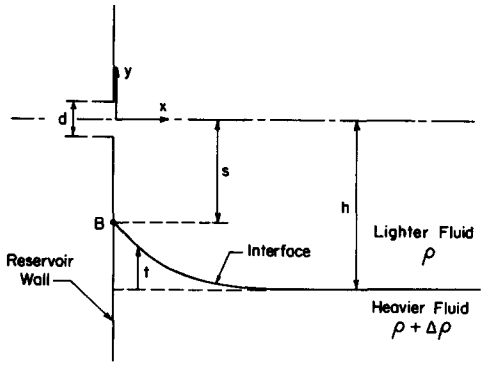

Figure 1 Schematic diagram of the flow situation

the present analysis follows Craya's[9] approach where equilibrium of the interface and the velocity field in the lighter fluid are determined first and then equality of the velocity and its gradient at linking point B (Figure 1) are later imposed as conditions for the onset of the phenomenon.

Equilibrium of the interface

Applying Bernoulli equation on a streamline coincident with the interface from the side of the lighter (moving) fluid, we get

$$P + \frac{\rho V^2}{2} + \rho g t = C \tag{4}$$

Along the same streamline from the side of the heavier (stationary) fluid, Bernoulli equation gives

$$P + (\rho + \Delta\rho) g t = C \tag{5}$$

subtracting Equation 5 from Equation 4, we get

$$\frac{V^2}{2} = \frac{\Delta\rho}{\rho} g t \tag{6}$$

Linking point B corresponds to the location on the interface where $t = h - s$. Therefore, the velocity at this point is given by

$$\frac{V_B^2}{2} = \frac{\Delta\rho}{\rho} g(h - s) \tag{7}$$

Velocity field in the lighter fluid

The presence of the stationary fluid is neglected in this part of the analysis. Therefore, the flow field of the lighter fluid is treated as a semi-infinite medium extending over $0 \leq x < \infty$ and $-\infty < y < \infty$, as shown in Figure 2. The medium is also

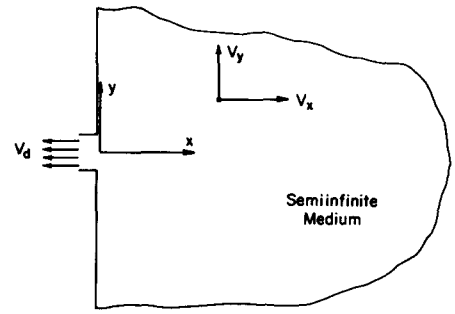

Figure 2 Flow domain of the lighter fluid

of infinite extent in the direction normal to the page. Flow within the medium is caused by a discharge with a uniform velocity V_d from the slot situated at $x = 0$ and $y = \pm d/2$. Consequently, we have a 2-D problem with V_x and V_y representing the velocity components in the x- and y-directions, respectively. Symmetry exists about the x-axis; therefore, the solution is required only for $0 \leq y < \infty$. Based on the assumptions stated earlier, the flow field within the medium can be derived from the potential flow theory.

Applying the continuity equation, we get

$$\frac{\partial V_x}{\partial x} + \frac{\partial V_y}{\partial y} = 0 \tag{8}$$

Introducing a scalar potential function ϕ, such that

$$V_x = \frac{\partial \phi}{\partial x} \quad \text{and} \quad V_y = \frac{\partial \phi}{\partial y} \tag{9}$$

we get the well-known Laplace equation

$$\frac{\partial^2 \phi}{\partial x^2} + \frac{\partial^2 \phi}{\partial y^2} = 0 \tag{10}$$

Equation 10 is subject to the following list of boundary conditions:

$$\left.\begin{aligned} \text{at } x = 0, \quad \frac{\partial \phi}{\partial x} &= -V_d, \quad 0 \leq y \leq \frac{d}{2} \\ &= 0, \quad y > \frac{d}{2} \end{aligned}\right\} \tag{11a}$$

$$\text{at } y = 0, \quad \frac{\partial \phi}{\partial y} = 0 \tag{11b}$$

$$\text{as } x \to \infty \text{ or } y \to \infty, \quad \phi \text{ is finite} \tag{11c}$$

A solution for Equation 10 satisfying boundary conditions 11b

Notation

C	Arbitrary constant used in Equations 4 and 5 (N/m^2)
d	Slot width (m)
f	Arbitrary function appearing in Equations 12–14 (m^3/s)
Fr	Froude number defined by Equation 3a
g	Gravitational acceleration (m/s^2)
h	Critical height (m)
P	Pressure (N/m^2)
q	Rate of discharge per unit slot length ($m^3/m.s$)
s	Distance defined in Figure 1 (m)
t	Distance defined in Figure 1 (m)
V	Local velocity (m/s)
V_d	Discharge velocity (m/s)
V_x	x-component of local velocity (m/s)
V_y	y-component of local velocity (m/s)
x, y	Coordinate system (m)

Greek symbols

$\Delta\rho$	Density difference between two fluids (kg/m^3)
η	Dimensionless parameter defined by Equation 27
λ	Eigenvalue (1/m)
ρ	Density (kg/m^3)
ϕ	Potential function (m^2/s)

and 11c can be written as

$$\phi = \int_0^\infty f(\lambda)\cos(\lambda y)e^{-\lambda x}\,d\lambda \tag{12}$$

where f is an arbitrary function. In order to determine f, we substitute the remaining boundary condition 11a into solution 12. Thus,

$$\left.\begin{aligned}\int_0^\infty \lambda f(\lambda)\cos(\lambda y)\,d\lambda &= V_d, \quad 0 \le y \le \frac{d}{2}\\ &= 0, \quad y > \frac{d}{2}\end{aligned}\right\} \tag{13}$$

Using Fourier cosine integrals, we obtain

$$\lambda f(\lambda) = \frac{2}{\pi}\int_0^{d/2} V_d\cos(\lambda y)\,dy$$

from which it is easy to obtain this formulation for the arbitrary function f,

$$f(\lambda) = \frac{2V_d}{\pi}\frac{\sin(\lambda d/2)}{\lambda^2} \tag{14}$$

Substituting Equation 14 into Equation 12, we get the following final formulation for the potential function within the field:

$$\phi = \frac{2V_d}{\pi}\int_0^\infty \frac{\sin(\lambda d/2)\cos(\lambda y)}{\lambda^2}e^{-\lambda x}d\lambda \tag{15}$$

The quantity that we are mainly interested in is the velocity component V_y along the wall ($x = 0$). This can be obtained by substituting Equation 15 into Equation 9, thus

$$V_y|_{x=0} = \left.\frac{\partial\phi}{\partial y}\right|_{x=0} = -\frac{2V_d}{\pi}\int_0^\infty \frac{\sin(\lambda d/2)\sin(\lambda y)}{\lambda}\,d\lambda \tag{16}$$

The integral in Equation 16 can be determined in closed form resulting in

$$V_y|_{x=0}/V_d = \frac{1}{\pi}\ln\left(\frac{y/d - 1/2}{y/d + 1/2}\right), \qquad |y/d| > 1/2 \tag{17}$$

It is to be noted that Equation 17 satisfies the condition of symmetry, i.e., $V_y|_{x=0}(y) = -V_y|_{x=0}(-y)$. Also, the edges of the slot ($y = \pm d/2$) are points of singularity that, fortunately, do not pose any problem in the subsequent analysis.

For comparison purposes, it is worthwhile to point out that the line-sink assumption adopted by Craya[9] results in the following velocity profile along the wall:

$$V_y|_{x=0}/V_d = -(1/\pi)/(y/d) \tag{18}$$

In exploring the effect of the slot dimension, Craya[9] suggested the following approximate velocity field based on the contraction of the emerging jet:

$$V_y|_{x=0}/V_d = -\left(\frac{1}{\pi}\right)\left[\left(\frac{y}{d}\right) + \left(\frac{2}{\pi+2}\right)\tan^{-1}\left(\frac{\pi}{\pi+2}\cdot\frac{V_y|_{x=0}}{V_d}\right)\right]^{-1} \tag{19}$$

Craya noted that the term distinguishing Equation 19 from Equation 18 diminishes as $|y/d|$ increases. Accordingly, velocity profile Equation 18 was used in developing correlations 1 and 2, with the understanding that these correlations are not affected by the dimension of the slot as long as h/d does not fall below 3 or 4.

Using the velocity profile given by Equation 17, the kinetic energy at linking point B, located at $x = 0$ and $y = -s$, can be expressed as

$$\frac{V_B^2}{2} = \frac{V_d^2}{2\pi^2}\left[\ln\left(\frac{s/d - 1/2}{s/d + 1/2}\right)\right]^2 \tag{20}$$

The critical height

We now have two expressions for $V_B^2/2$, given by Equations 7 and 20, applicable at point B, which links the interface with the wall of the reservoir. Figure 3 shows a graphic representation of these two expressions for fixed values of V_d, g, ρ, $\Delta\rho$, and d. Under these conditions, Equation 20 provides a specific relation between $V_B^2/2$ and s represented by the curve in Figure 3, while Equation 7 produces a set of parallel straight lines whose locations depend on the value of h. For large values of h, the straight line and the curve do not intersect, while two points of intersection are possible with small values of h. There is one value of h that produces a single intersection with the straight line given by Equation 7 forming a tangent to the curve given by Equation 20. The hypothesis in this analysis (similar to Craya[9]) is that this value of h corresponds to the critical height for the onset of liquid entrainment and it can be determined by equating $V_B^2/2$ given by Equations 7 and 20 and their first derivative with respect to s. Accordingly, at the onset of liquid entrainment, we have

$$\frac{\Delta\rho}{\rho}g(h - s) = \frac{V_d^2}{2\pi^2}\left[\ln\left(\frac{s/d - 1/2}{s/d + 1/2}\right)\right]^2 \tag{21}$$

and

$$-\frac{\Delta\rho}{\rho}g = \frac{V_d^2}{d\pi^2}\left[\ln\left(\frac{s/d - 1/2}{s/d + 1/2}\right)\right]\left[\frac{1}{(s/d)^2 - 1/4}\right] \tag{22}$$

Nondimensionalizing, using definition 3a for Froude number, the following final correlations can be developed

$$\frac{h}{d} - \frac{s}{d} = \frac{1}{2}\left(\frac{\mathrm{Fr}}{\pi}\right)^2\left[\ln\left(\frac{s/d - 1/2}{s/d + 1/2}\right)\right]^2 \tag{23}$$

and

$$\ln\left(\frac{s/d + 1/2}{s/d - 1/2}\right) = \frac{(s/d)^2 - 1/4}{(\mathrm{Fr}/\pi)^2} \tag{24}$$

Equations 23 and 24 provide the necessary relations for determining h/d and s/d corresponding to any given value of Fr. This interesting feature, whereby both h/d and s/d are dependent only on Fr, is similar to Equations 1 and 2. With a given Fr, an iterative procedure is necessary for determining s/d from Equation 24, which is then substituted in Equation

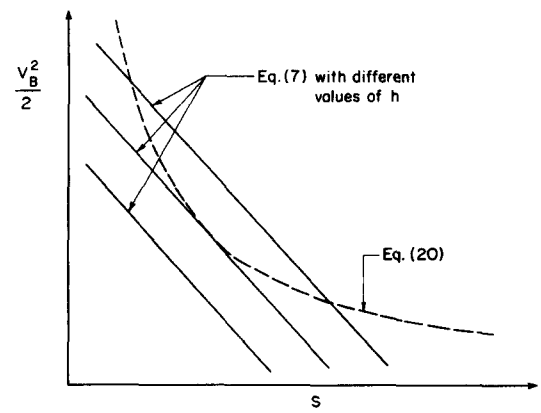

Figure 3 Behavior of $V_B^2/2$ *versus* s

23 for evaluating h/d. It can be easily verified from these equations that both s/d and h/d approach the limiting value of 1/2 as Fr approaches zero. As Fr increases, the predictions of Equations 23 and 24 gradually approach those of Equations 1 and 2, as shown later.

Following the procedure outlined previously, correlations of the onset of liquid entrainment were also developed using velocity profile 19 suggested by Craya.[9] Details of the derivation are not presented here; however, the final result is given by the following dimensionless relations:

$$\frac{h}{d}-\frac{s}{d}=\frac{\eta}{2\pi}\left[\frac{(\pi+2)^2\eta^2-\pi^2}{(\pi+2)^2\eta^2+\pi^2}\right] \tag{25}$$

and

$$\frac{s}{d}=\frac{\eta}{\pi}+\frac{2}{\pi+2}\tan^{-1}\left(\frac{\pi}{\pi+2}\cdot\frac{1}{\eta}\right) \tag{26}$$

where

$$\eta=\mathrm{Fr}\left[2\left(\frac{h}{d}-\frac{s}{d}\right)\right]^{-1/2} \tag{27}$$

Specifying a value for η, s/d can be determined from Equation 26, h/d from Equation 25, and Fr from Equation 27. Therefore, s/d and h/d are both dependent only on Fr, similar to the model given by Equations 23 and 24. The lower limit $\eta = \pi/(\pi+2)$ corresponds to $s/d = h/d = 1/2$ and Fr = 0.

Numerical results and discussion

Using the equations derived previously, computations were made in order to illustrate the effect of the slot width. Figure 4 shows the three velocity profiles ($V_y|_{x=0}/V_d$) given by Equations 17–19 along the wall underneath the slot. Beyond $|y/d|$ of about 2.5, the three profiles are practically identical. The deviation between the profile developed in the present analysis (Equation 17) and the one suggested by Craya[9] is very small for all y/d. It is the difference between the present velocity profile and the one corresponding to the line-sink assumption over the zone $0.5 < |y/d| < 2.5$ that is significant for this study.

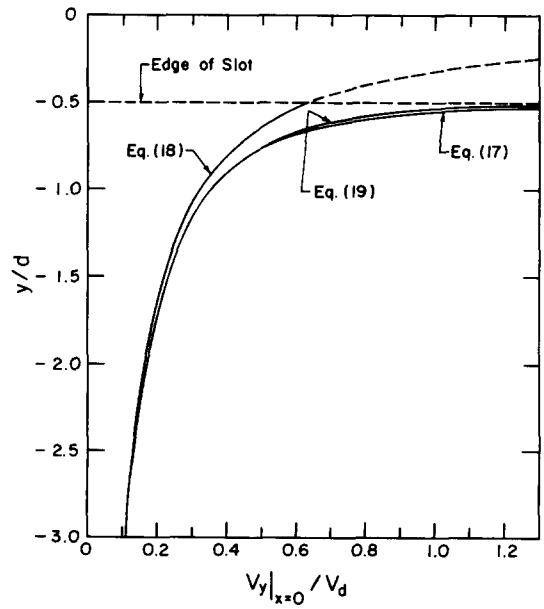

Figure 4 Velocity profiles along the wall underneath the slot

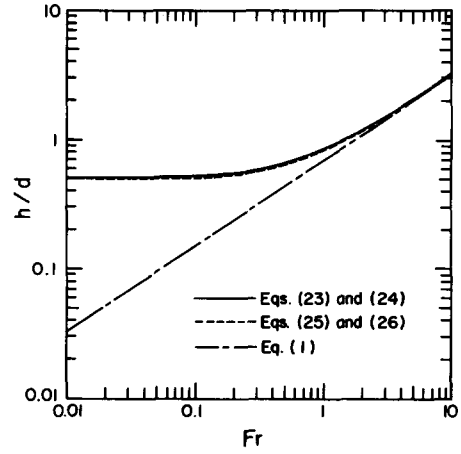

Figure 5 Variation of h/d with Fr

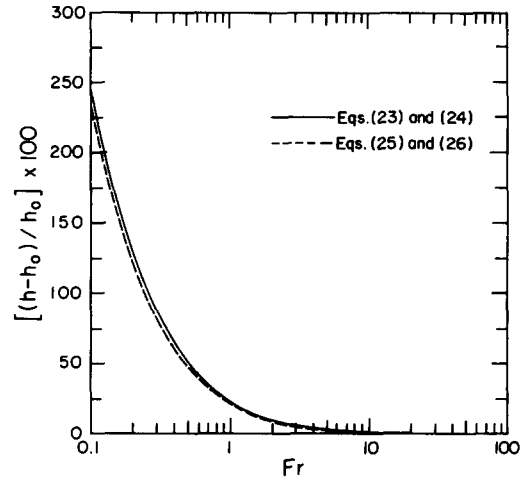

Figure 6 Percentage deviation from Craya's[9] model

Figure 5 shows the behavior of h/d as a function of Fr. The present model, given by Equations 23 and 24, and the model derived from Craya's[9] suggested velocity profile, given by Equations 25 and 26, produce nearly identical results. Both of these models approach the physically appropriate limit of $h/d = 0.5$ at Fr = 0, and they converge to the simplified model given by Equation 1 at larger Fr. The deviation between the present model and Equation 1 is quantified in Figure 6. In this figure, h_0 refers to the value of h calculated from Equation 1. The magnitude of this deviation is about 244 percent at Fr = 0.1, 22.8 percent at Fr = 1, and 1.2 percent at Fr = 10. Beyond Fr = 10, which corresponds to $h/d = 3.28$ and $s/d = 2.22$, the error in using Equations 1 and 2 is negligible. This value of s/d is consistent with Figure 4, which shows small differences in the velocity profiles beyond $|y/d|$ of about 2.2.

For completeness, the variation of s/h with Fr is presented in Figure 7. This ratio approaches one as Fr approaches zero and converges to 2/3 for Fr > 10.

The possibility of comparing the present theoretical predictions with published experimental data was given careful consideration. As mentioned earlier, the results[2–8] pertain to circular orifices and, therefore, cannot be compared with the present analysis. The only experimental investigation, to the authors' best knowledge, in which the present break geometry of a horizontal slot was considered is the one by Gariel.[10]

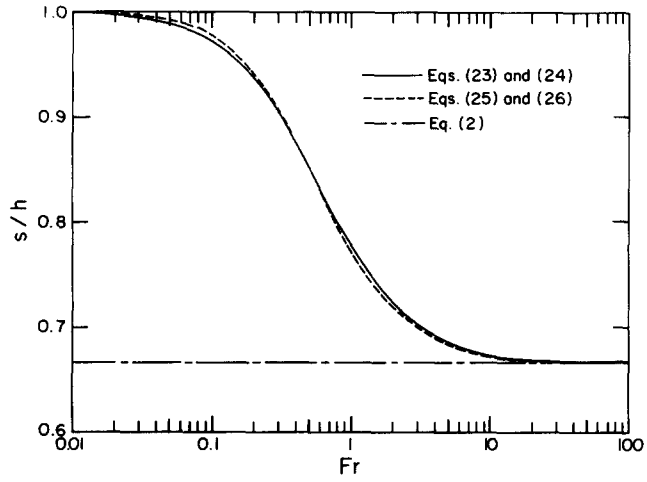

Figure 7 Variation of s/h with Fr

Unfortunately, Gariel did not report the slot width d used in his experiment, which is a crucial parameter in the present analysis. The results were reported graphically in terms of h *versus* $q\sqrt{\Delta\rho}$.[10] Without knowing d, the Froude number cannot be determined and the present model given by Equations 23 and 24 cannot be solved. Further experiments are recommended for this important break geometry.

Concluding remarks

A commonly used model for the prediction of the onset of liquid entrainment from side slots is the one developed by Craya[9] and given by Equations 1 and 2. This model was simplified by treating the slot as a 2-D line sink. The present analysis extends Craya's model[9] to slots of finite width and succeeds in developing simple algebraic equations for predicting the critical height h. One interesting feature of the present model is that, irrespective of the width of the slot d, the ratios h/d and s/d are dependent only on Froude number. Also, beyond Fr = 10 the present model closely approaches Craya's simplified model.[9] However, the present model is recommended for Fr < 10 where it is demonstrated that significant deviations exist between the two models.

Acknowledgment

The financial assistance provided by the Natural Sciences and Engineering Research Council of Canada is gratefully acknowledged.

References

1 Zuber, N. Problems in modeling of small break LOCA. *Nuclear Regulatory Commission*, Report No. NUREG-0724, 1980

2 Crowley, C. J., and Rothe, P. H. Flow visualization and break mass measurements in small break separate effect experiments. *ANS Specialist Meeting on Small Break Loss of Coolant Accident Analyses in LWR's*, Monterey, CA, USA, 25–27 August, 1981

3 Smoglie, C., and Reimann, J. Two-phase flow through small branches in a horizontal pipe with stratified flow. *Int. J. Multiphase Flow*, 1986, **12**, 609–625

4 Smoglie, C., Reimann, J., and Muller, U. Two-phase flow through small breaks in a horizontal pipe with stratified flow. *Nucl. Eng. Des.*, 1987, **99**, 117–130

5 Schrock, V. E., Revankar, S. T., Mannheimer, R., Wang, C.-H., and Jia, D. Steam-water critical flow through small pipes from stratified upstream regions. *Proc. 8th Int. Heat Transfer Conf.*, 1986, **5**, 2307–2311

6 Micaelli, J. C., and Memponteil, A. Two phase flow behavior in a tee-junction: the CATHARE model. *Proc. 4th Int. Topical Meeting on Nuclear Reactor Thermal-Hydraulics*, 1989, **2**, 1024–1030

7 Gardner, G. C. Co-current flow of air and water from a reservoir into a short horizontal pipe. *Int. J. Multiphase Flow*, 1988, **14**, 375–388

8 Yonomoto, T., and Tasaka, K. New theoretical model for two-phase flow discharged from stratified two-phase region through small break. *J. Nucl. Sci. Tech.*, 1988, **25**, 441–455

9 Craya, A. Theoretical research on the flow of non-homogeneous fluids. *La Houille Blanche*, 1949, **4**, 44–55

10 Gariel, P. Experimental research on the flow of non-homogeneous fluids. *La Houille Blanche*, 1949, **4**, 56–64